Choi *et al.*
Journal of Analytical Science and Technology (2024) 15:13
https://doi.org/10.1186/s40543-024-00426-4

Journal of Analytical Science and Technology

SHORT REPORT

Open Access

Microstructural and microchemical analysis of zircon in a syenite lithic fragment from Ulleung Island volcano, South Korea

Seungsoon Choi[1], Keewook Yi[1], Haemyeong Jung[2] and Albert Chang-sik Cheong[1*]

Abstract

Background The intricate textural patterns commonly observed in metamorphosed and recrystallized zircon ($ZrSiO_4$) underscore the crucial necessity of understanding the underlying mechanisms governing their formation to ensure accurate interpretation of the chemical and isotope data they contain. This study employed a combination of microanalytical techniques, including electron backscattered diffraction (EBSD) analysis, electron microprobe (EMP) mapping, and scanning electron microscope (SEM) imaging, to investigate the processes of formation and modification of zircon in a late Pleistocene (~ 35 ka) syenite enclosed within the Nari Tephra Formation on Ulleung Island in South Korea.

Findings Under cathodoluminescence (CL), zircons within the syenite reveal dark, featureless, or oscillatory-zoned cores containing numerous inclusions of britholite. These cores are partially or entirely replaced by inward-penetrating bright-CL domains that exhibit minimal inclusion presence. Despite these changes, the external morphologies of the zircons remain largely unchanged, and the faded oscillatory zoning is preserved in the replaced regions. EMP mapping discloses amoebiform micro-domains with high Y, U, and Th concentrations within the dark-CL cores, while the bright-CL domains are relatively deficient in these trace elements. Microstructural analysis of the zircons using EBSD mapping indicates no significant misorientation between the dark-CL cores and the bright-CL rims. Deformation-related low-angle boundaries by lattice distortion are clearly observed in certain grains, cutting across the discrete SEM and EMP domains, and often aligned along submicron pore trails.

Conclusions Microstructural and microchemical analyses carried out in this study establish that the zircons within the Ulleung syenite have undergone subsolidus recrystallization, a process likely influenced by the presence of fresh melts or fluids. This recrystallization process could be attributed to either coupled dissolution and reprecipitation or thermoactivated particle and defect volume diffusion due to inherent lattice strain. The subsequent deformation observed in the zircons might be a result of increased stress within the magma system after the recrystallization.

Keywords Zircon, Ulleung Island, Recrystallization, Deformation, SEM, EBSD, EMP

Introduction

The mineral zircon ($ZrSiO_4$) has garnered significant attention in the fields of geochronology and geochemistry due to its remarkable capacity to preserve critical details regarding the nature and timing of past geological events. The enduring nature of zircon is primarily attributed to the limited volume diffusion of its constituent ions, even under conditions approaching magmatic temperatures (Cherniak and Watson 2003). Zircon's

*Correspondence:
Albert Chang-sik Cheong
ccs@kbsi.re.kr
[1] Korea Basic Science Institute Ochang Center, Cheongju 28119, Republic of Korea
[2] School of Earth and Environmental Sciences, Seoul National University, Seoul 08826, Republic of Korea

exceptional durability has also positioned it as a promising candidate for the disposal of radioactive waste (Ewing et al. 1995).

However, the presence of intricate secondary internal textures commonly observed in metamorphosed and recrystallized zircons (Corfu et al. 2003; Rubatto 2017) indicates that the primary zircon crystals were not always impervious to environmental changes. This is typically manifested by the replacement of initially zoned zircon with unzoned counterparts. Several distinct mechanisms have been put forward to elucidate this textural modification: (1) thermoactivated particle and defect volume diffusion in which lattice strain is reduced by the expulsion of large-radius trace elements (Hoskin and Black 2000), (2) dry thermal annealing of self-irradiated zircon leading to the structural recovery of metamict amorphized zircon (Geisler 2002), (3) diffusion–reaction process wherein a hydrous species diffuses inward, catalyzing the structural recovery of metamict zircon (Geisler et al. 2007), and (4) coupled dissolution-reprecipitation processes linked to the thermodynamics of solid solution-aqueous solution system (Geisler et al. 2007). Trace elements are redistributed in zircon as a consequence of any (or any combination) of these processes. Alternatively, elemental diffusion could be modified by the presence of deformation-related microstructures in zircon (Reddy et al. 2006; Timms et al. 2011; Piazolo et al. 2016). The precise nature of trace element redistribution has long been a topic of debate (Pidgeon et al. 1998; Hoskin and Black 2000; Reddy et al. 2006; Geisler et al. 2007; Timms et al. 2011; Piazolo et al. 2016; Huijsmans et al. 2022).

It has been conventionally believed that the secondary modification of zircon could be easily identified through cathodoluminescence (CL) observation. However, it is noted that CL emission and suppression in zircon are primarily influenced by concentrations of some specific elements and defect centers (Hanchar and Rudnick 1995; Rubatto and Gebauer 2000; Poller et al. 2001; Nasdala et al. 2002). Electron backscattered diffraction (EBSD) analysis of deformed zircon might reveal intragrain misorientations and orientation boundaries that are not easily discerned in CL images (Reddy et al. 2006, 2009). These boundaries bear geochronological and geochemical significance, serving as efficient pathways for the diffusion of trace elements and U–Pb isotopes (Piazolo et al. 2016).

The purpose of this study is to provide a detailed description of the internal structures within zircon from a Quaternary syenite lithic fragment on Ulleung Island in Republic of Korea. This investigation employs a combination of EBSD and electron microprobe (EMP) mapping, alongside conventional CL and backscattered electron (BSE) imaging. The selection of this particular zircon is based on its young crystallization age, ensuring efficient elimination of self-irradiation effects when interpreting the observed textural images and trace element distribution.

Materials and methods

The study material was gathered from Ulleung Island, Republic of Korea (37°30′16.0′′N, 130°51′45.2′′E), an emergent peak of a Quaternary alkaline magma system behind the Japan Arc (Fig. 1a). This island elevates about 3,000 m above the seafloor, with the exposed section reaching a peak of 982 m and covering an area of 72.6 km^2. The island's landscape was significantly shaped by explosive eruptions that began earnestly in the latest Pleistocene, around 19 ka (Kim et al. 2014), and crafted an amphitheater-shaped caldera named Nari at the island's center. These volcanic activities led to the accumulation of the trachytic/phonolitic sequence named as the Nari Tephra Formation (Kim et al. 2014). Throughout these eruption events, significant lithic fragments of gabbro, monzonite, and syenite were transported to the surface. The zircons under investigation in this study were obtained from a syenite—a white–gray and partly pegmatitic rock (Fig. 1b). This syenite is composed of K-feldspar (~70%), hornblende (10%), plagioclase (10%), clinopyroxene (5%), and biotite (5%), and it features numerous tourmaline crystals that extend to several centimeters in length. K-feldspar in the sample exhibits subhedral, and is dominated by micro-sized pores (Fig. 1c, d). The zircon grains are observed on grain boundaries between constituent minerals (Fig. 1d). The zircon grains were separated from syenite by crushing, sieving, magnetic, heavy liquid, and hand-picking techniques (Cheong et al. 2013). The separated zircon grains exhibit transparency or a pale brown hue, and their crystal faces are euhedral to subhedral, reaching lengths of up to 250 μm. They yielded a weighted mean U-Th age of 34.7 ± 2.3 ka, which represents the crystallization timing (Cheong et al. 2024).

For the microstructural and microchemical analysis, the separated zircon grains were mounted using epoxy, and polished with diamond paste and colloidal silica (Syton). Finally, the polished surface of the sample was coated with carbon to prevent charging in a scanning electron microscope (SEM). The surfaces of zircons were characterized by BSE and CL imaging using a field emission scanning electron microscope (FE-SEM, JEOL JSM 7100F) at the School of Earth and Environmental Sciences (SEES) in Seoul National University (SNU), Republic of Korea and a SEM (JEOL JSM-6610LV) at the Korea Basic Science Institute (KBSI), respectively. EBSD mapping was conducted to measure crystallographic orientation of zircon grains and whole rock using the FE-SEM (JEOL JSM 7100F) equipped with an

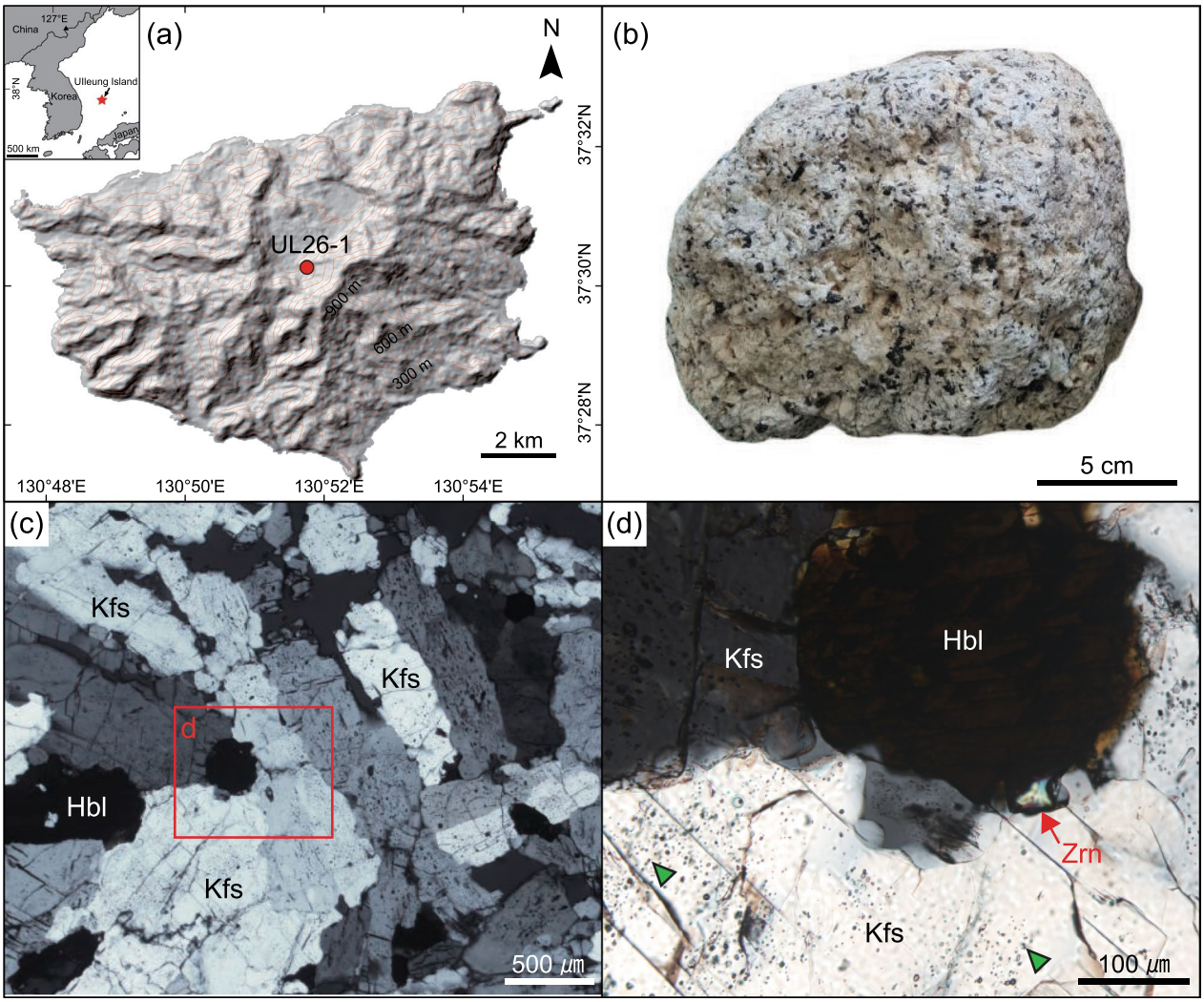

Fig. 1 **a** Digital elevation model of Ulleung Island derived from ASTER satellite data captured on 30 November 2013, illustrating the topography and indicating the sample site. The inset figure indicates the geographic position of Ulleung Island. **b** Photograph of the syenite rock specimen. **c** Optical photomicrograph of the syenite sample in cross-polarized light. The red box indicates the location of the area displayed in (**d**). **d** Enlarged optical photomicrograph of the syenite sample showing zircon in cross-polarized light. Green arrowheads indicate pore trails in K-feldspar. Kfs: K-feldspar, Hbl: hornblende, Zrn: zircon

Oxford Symmetry detector at SEES in SNU. The EBSD system was operated at a 20 kV acceleration voltage, a 10 nA probe current, a 25 mm working distance, a 9.6×10^{-5} Pa vacuum, and 70° sample tilt. EBSD patterns of zircons were collected automatically using 0.1–0.2 μm step sizes. The raw EBSD data were cleaned using AZtec software (Version 6.0) through the following steps: (1) removal of pixel-sized wild spikes, (2) removal of non-indexed pixels neighboring indexed six pixels, and (3) removal of pixel-sized wild spikes. Band contrast (BC) and grain reference orientation deviation (GROD) maps of individual zircon grains were created using AZtecCrystal software. BC maps show microstructures such as grain boundaries and subgrain boundaries and indicate roughly a degree of crystallinity based on a measure of the intensity of the indexed Kikuchi bands (Claves and Deal 2005). GROD maps show intracrystalline deformation in grains and are generated by determination of deviation between the average orientation of the grain and the orientation of each pixel in the grain. EMP mapping was conducted to obtain elemental maps for Y, Hf, U, Yb, Th, and Zr of zircon grains using JEOL JXA-8100. The EMP system was operated at a 15 kV acceleration voltage, a 250 nA

probe current, 200 ms dwell time, and 0.6–0.8 μm step sizes.

Results

BSE and CL observations

CL images of the representative zircon grains are shown in Fig. 2. BSE images of five grains are provided in Fig. 3 with their CL images. The BSE images show bright, featureless, or convoluted zoned cores. The cores usually contain inclusions of britholite. Oscillatory zoning within zircon is occasionally observed in the CL and BSE image (Figs. 2 and 3). Dark domains with straight or curved boundaries are frequently observed, extending from the rims to the cores or throughout the entire grains in the BSE images (Fig. 3c–e). Micro-sized pores are typically seen as remnants of detached inclusions (Fig. 3a–c), while submicron pores are mostly found along the boundaries of the dark domains (Fig. 3d, e) in the BSE images. Amoebiform micro-domains surrounding concentrated micro-sized pores and inclusions appear bright in the BSE images (Fig. 3b, c). In the CL images of the zircons (Figs. 2 and 3), distinct luminescence patterns are observed. Dark, featureless, or oscillatory-zoned cores containing the numerous inclusions are partially or entirely replaced by inward-penetrating bright-CL domains that exhibit the minimal inclusion presence (Figs. 2 and 3). Despite these changes, the external morphologies of the zircons remain largely unchanged, and the faded oscillatory zoning is preserved in some replaced domains (Figs. 2 and 3a–c).

EBSD analysis

Figure 3 presents the EBSD mapping results for the representative five zircon grains in the form of BC and GROD maps. These maps reveal various textural features within the zircon grains. The zircon grains exhibit a featureless texture (Fig. 3b) or the presence of low-angle subgrain boundaries and gradual lattice bending (Figs. 3c–e and 4). The low-angle boundaries are typically straight or curved, extending from the rims to the cores or across the entire grains. They often align with the boundaries of dark domains observed in the BSE images (Fig. 3c–e) and frequently correspond to the trails of submicron pores (Fig. 3d, e). Notably, these low-angle boundaries do not seem to correlate with the bright or dark domains observed in the CL images (Fig. 3c–e). The maximum misorientations of these low-angle boundaries are typically within 2°. In contrast to other grains, grains A1 and A13 exhibit lattice distortion primarily caused by fractures, rather than intracrystalline deformation (Fig. 3a, e). These fractures are distinctly identified as black lines in both the BSE images and BC maps. Based on the BC

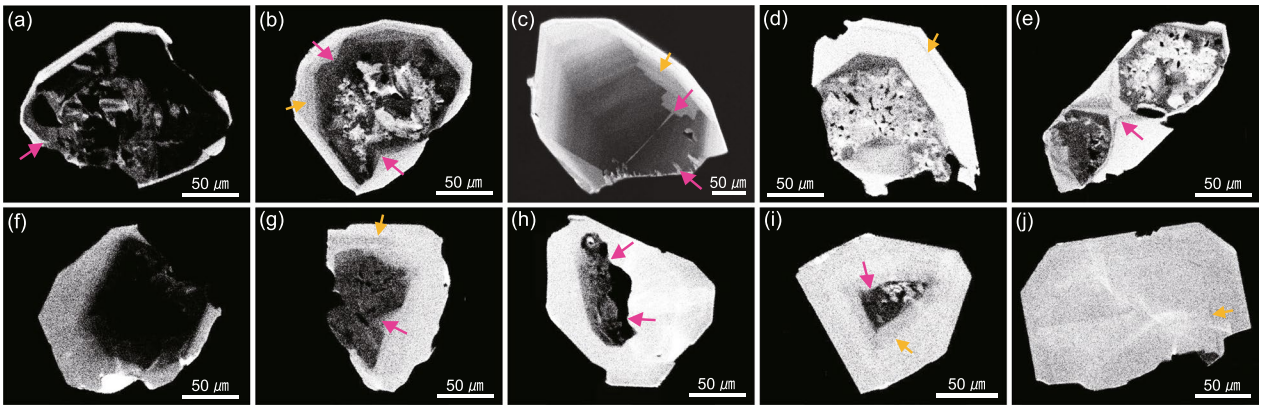

Fig. 2 CL images of zircon grains. The dark-CL cores within the grains are partially or entirely replaced by bright-CL domains. The images are arranged sequentially **a**–**j** based on the degree of recrystallization. Orange arrows highlight faded oscillatory zoning. Pink arrows indicate inward-penetrating features of bright-CL domains

(See figure on next page.)

Fig. 3 Microstructural and microchemical analyses of zircon using BSE and CL images, as well as BC, GROD, and EMP maps of trace elements and zirconium in grain A1 (**a**), grain A3 (**b**), grain A6 (**c**), grain A9 (**d**), and grain A13 (**e**). Green arrowheads indicate fractures, possibly formed during laser ablation in a separate study or during zircon separation. Blue arrowheads mark the spots analyzed by laser ablation. Red boxes represent the areas of EMP mapping. Yellow arrowheads depict submicron pore trails along low-angle boundaries. Black arrows point to a recrystallization front. Orange arrows denote faded oscillatory zoning, and pink arrows indicate inward-penetrating features of bright-CL domains. Red arrowheads highlight low-angle boundaries. The white box in **e** signifies the location of Fig. 4a. Y: yttrium, Hf: hafnium, U: uranium, Yb: ytterbium, Th: thorium, Zr: zirconium

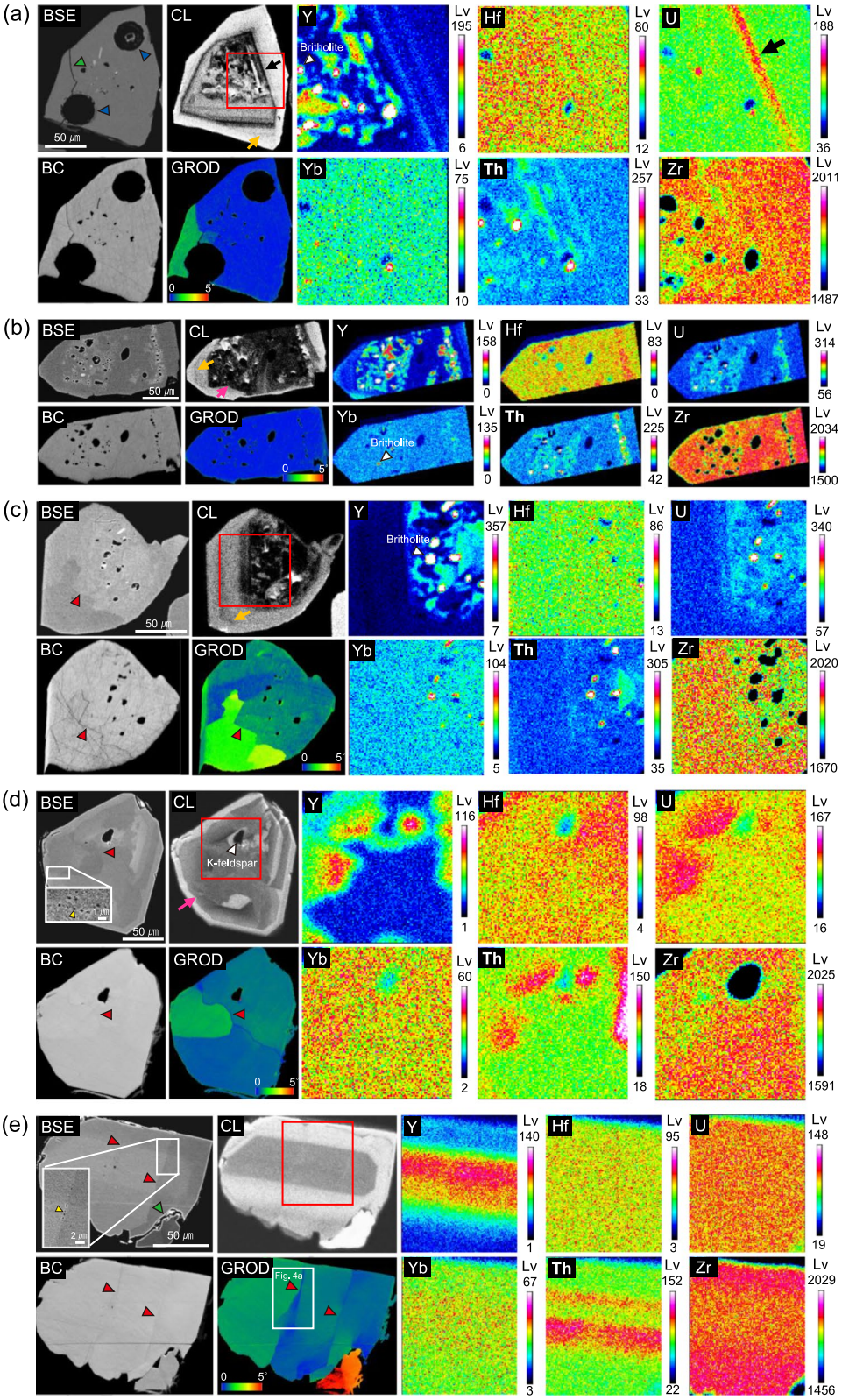

Fig. 3 (See legend on previous page.)

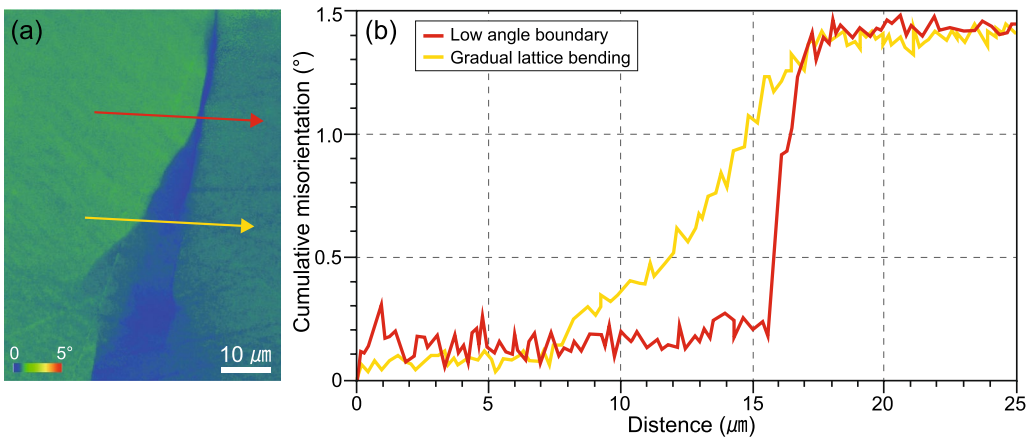

Fig. 4 **a** Enlarged GROD map of grain A13 showing both low-angle boundary and gradual lattice bending in the upper part and lower part of the map, respectively. The red and yellow lines in (**a**) indicate location of cumulative misorientation profiles shown in (**b**). **b** Cumulative misorientation profiles for the red and yellow lines shown in (**a**). The red line illustrates the low-angle boundary with steep lattice distortion, while the yellow line represents the gradual lattice bending with continuous lattice distortion

maps, there is no clear change in crystallinity between the distinct CL domains in each zircon.

EMP analysis

In Fig. 3, we present elemental maps illustrating the relative concentrations of trace elements (Y, Hf, U, Yb, and Th) and Zr within the representative five zircon grains. Amoebiform micro-domains enriched in Y, U, and Th are usually observed within the dark-CL cores and near inclusions (Fig. 3). The britholite inclusions are well highlighted in Y, U, Yb, and Th maps. In grain A1, a line of Y, U, and Th enrichment corresponds to the boundary between the dark core and bright rim in the CL image (Fig. 3a). In contrast, grain A13, which lacks inclusions, displays the enrichment of Y and Th within the dark-CL core, with the bright-CL domain relatively deficient in these trace elements (Fig. 3e). Yb and Hf show minimal variation within the zircons compared to other trace elements. In contrast, the concentration of Zr appears to behave inversely to that of Y, U, and Th within the zircons.

Discussion

Recrystallization of zircon

Most zircon grains examined in this study reveal dark-CL cores characterized by weak or clear oscillatory zoning (Figs. 2 and 3) indicating a typical magmatic texture possibly related to ordering in the melt by polymerization (Hoskin 2000). The cores contain numerous inclusions (Fig. 3) and are partially or entirely replaced by inward-penetrating bright-CL rims devoid of inclusions, with no significant change in external morphology (Figs. 2 and 3). Remarkably, the faded oscillatory zoning is preserved in some replaced regions. Additionally, the concentrations of trace elements (Y, U, and Th) are higher in the dark-CL cores than in the bright-CL rims (Fig. 3). These findings suggest that the zircon grains have undergone subsolidus recrystallization. It is noted that we adopt the term defined by Rubatto (2017), where recrystallization, another term for replacement, is described as "an in situ process that alters the chemical (and possibly isotopic) composition of an existing domain, occurring under subsolidus conditions."

Considering the young crystallization age of the zircons in this study (34.7 ± 2.3 ka) (Cheong et al. 2024), it is unlikely that self-irradiation effects are responsible for this textural modification. Thus, we explore other mechanisms for the recrystallization based on microstructural and microchemical observations. Hoskin and Black (2000) proposed that zircon recrystallization can result from thermoactivated particle and defect volume diffusion, whereby lattice strain is reduced by the expulsion of large-radius trace elements. CL images of zircon grains in their study show secondary internal structures, including faded oscillatory zoning, transgressive recrystallization, and recrystallization fronts that cross-cut primary igneous zoning and cores. These recrystallization fronts are characterized by enriched trace elements expelled from the recrystallized zones. Moreover, there are consistent EBSD patterns with no misorientation between the primary and recrystallized zones in zircon grains. In our study, grain A1 exhibits enriched trace elements (Y, U, and Th) in the recrystallized front, with no misorientation between the distinct core and rim (Fig. 3a). The faded oscillatory zoning is also observed in the recrystallized rim of this grain. These findings, consistent with

those in Hoskin and Black (2000), suggest that this zircon grain might have undergone recrystallization through thermoactivated particle and defect volume diffusion. However, other grains do not display enriched trace elements in the recrystallized fronts.

Alternatively, the recrystallized zircon grains might result from a coupled dissolution-reprecipitation process linked to the thermodynamics of the solid solution-aqueous solution system (Geisler et al. 2007). This mechanism is characterized by lower trace element concentrations, such as U and Th, in recrystallized domains compared with primary domains. It is also characterized by the formation of inward-moving interfaces, pores, and inclusions (such as thorite and xenotime) in the recrystallized domains. Therefore, this mechanism may lead to the formation of chemically purer zircon in the reprecipitated domain compared to the primary domain (Geisler et al. 2007; Vonlanthen et al. 2012). In our study, the zircon grains exhibit textures akin to those resulting from the coupled dissolution-reprecipitation process, but they lack pores and inclusions in the recrystallized domains (Fig. 3b–e). The absence of pores and inclusions in the recrystallized domains may be due to textural equilibration and the non-attainment of a "eutectic" point causing the precipitation of inclusions in the thermodynamics of solid solution–aqueous solution systems (Geisler et al. 2007).

The exact causes of the recrystallization process are challenging to pinpoint. However, recent oxygen isotope data offer one perspective on this phenomenon. In a previous study (Cheong et al. 2024), a significant increase in $\delta^{18}O$ toward the recrystallized bright-CL rims was observed, suggesting the rejuvenation of magma reservoirs through the injection of new melt or fluid. This rejuvenation likely acted as a trigger for the explosive eruptions on Ulleung Island. The recrystallization process of the zircons in this study may be attributed to either thermoactivated particle and defect volume diffusion or coupled dissolution and reprecipitation, which may have been influenced by this rejuvenation.

Relationship between low-angle boundaries and trace element distribution

Within deformation-related microstructures of zircon, low-angle boundaries are often regarded as efficient conduits for the diffusion of trace elements and radiogenic isotopes (Reddy et al. 2006; Timms et al. 2011; Piazolo et al. 2016). Reddy et al. (2006) demonstrated the enrichment of rare earth elements (REEs) toward zircon tips where low-angle boundaries are concentrated, employing sensitive high-resolution ion microprobe (SHRIMP) and EBSD techniques. Timms et al. (2011) reported not only enrichment in REEs, U, and Th but also the depletion of Ti at low-angle boundaries in zircon grains, using panchromatic CL, SHRIMP, and EBSD techniques. In addition, Piazolo et al. (2016) exhibited enriched trace elements (Y, U, and Al) at a low-angle boundary within a zircon grain on a nanometer scale, employing atom probe tomography and EBSD techniques.

In contrast, our study reveals almost indistinguishable change in trace element patterns at the low-angle boundaries in the zircon grains (Fig. 3c–e). Furthermore, the low-angle boundaries overprint the recrystallized domains in the zircon grains. These findings suggest that the recrystallization took place before the deformation, and it appears that trace element diffusion at the low-angle boundaries had not yet occurred after the deformation in the zircons.

Formation of deformation microstructures

In this study, we observe deformation-induced low-angle boundaries and gradual lattice bending in certain zircon grains extracted from the syenite (Figs. 3c–e and 4). Fractures are absent at these low-angle boundaries in both BSE images and BC maps. These observations suggest that some of the zircon grains may have undergone plastic deformation, a finding consistent with previous studies that utilized EBSD analysis on various rock types, including gabbro (Reddy et al. 2006), andesite (Reddy et al. 2009; Timms et al. 2012), gneiss (Piazolo et al. 2016), granulite-facies, and amphibolite-facies rocks (Kovaleva et al. 2017).

Low-angle boundaries in the zircon grains in this study often exhibit submicron pore trails (Fig. 3d, e). This suggests that the deformation leading to the formation of low-angle boundaries may have been triggered by increased stress, particularly concentrated around pre-existing pores in the zircon grains. Stress localization around pores can induce lattice distortion within zircon (Timms et al. 2012). Alternatively, submicron pores might result from cavitation induced by the coalescence of migrating dislocations at low-angle boundaries in zircon (Timms et al. 2012). Submicron cavities can accumulate at grain boundaries due to dislocation pile-ups and are referred to as Zener-Stroh cracks (Stroh 1957; Weertman 1986). Low-angle boundaries may act as interfaces that impede the migration of dislocations (Précigout et al. 2022). Consequently, the submicron pores in the zircons in this study may also have been formed due to plastic deformation resulting from the development of low-angle boundaries.

Moreover, in the syenite sample as a whole rock, we observe prevalent intracrystalline deformation in K-feldspar grains through optical photomicrography and EBSD maps (Fig. 5). These K-feldspar grains exhibit undulose extinction in cross-polarized light (Fig. 5a) and display

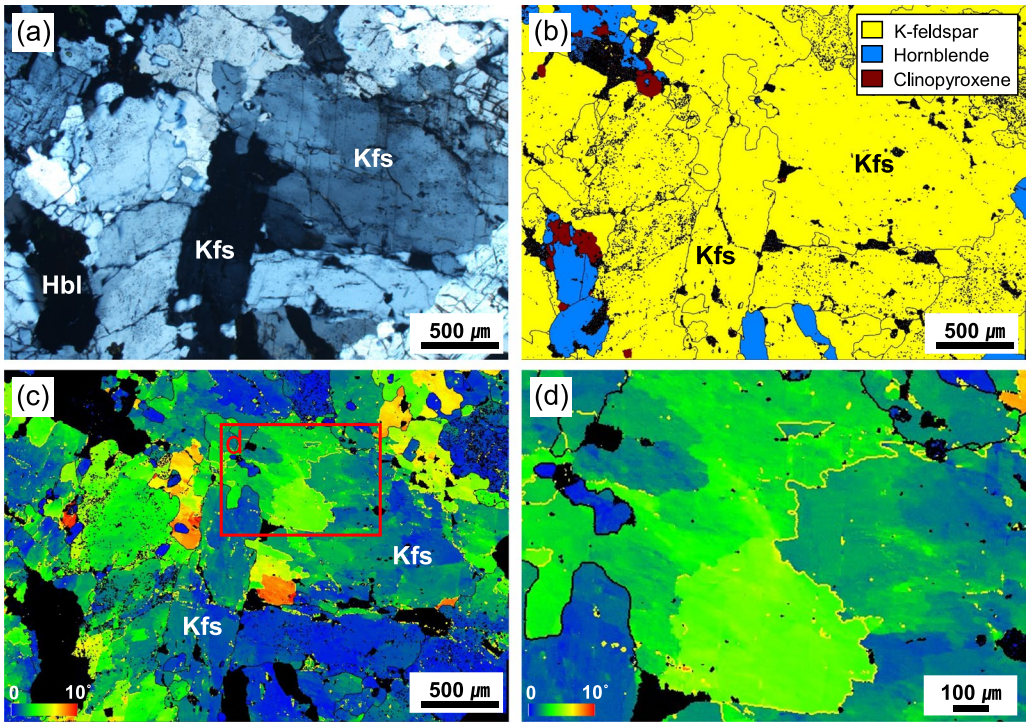

Fig. 5 **a** Optical photomicrograph of the syenite sample showing undulose extinction in K-feldspar in cross-polarized light. **b** EBSD phase map of the syenite sample. **c** GROD map of K-feldspar in the syenite sample. Black lines indicate grain boundaries. Yellow lines indicate subgrain boundaries by misorientation ranged from 2° to 10°. The red box indicates the location of the area displayed in (**d**). **d** Enlarged GROD map of K-feldspar in the syenite sample showing intracrystalline deformation. The EBSD patterns were collected automatically using a step size 3 μm. Kfs: K-feldspar, Hbl: hornblende

subgrain boundaries and intracrystalline misorientations in the GROD map (Fig. 5c, d). These observations provide strong evidence of plastic deformation in the whole rock. Thus, the plastic deformation is observed not only in some zircon grains but also in the whole rock. Since the deformation in the zircons may have occurred after the recrystallization, the deformation observed at the whole-rock scale might be the result of increased stress within the magma system subsequent to the recrystallization of zircon.

Concluding remarks

This study investigated the microstructural and microchemical processes of zircons within the syenite lithic fragment from Ulleung Island volcano, employing a combination of EBSD and EMP mapping, in addition to conventional CL and BSE imaging techniques. The findings reveal that the zircons have undergone subsolidus recrystallization, likely influenced by the presence of fresh melts or fluids. This recrystallization process could be attributed to either thermoactivated particle and defect volume diffusion or coupled dissolution and reprecipitation. Low-angle boundaries in the zircons, which exhibit negligible changes in trace element patterns and intersect the recrystallized domains, suggest that deformation may have occurred subsequent to the recrystallization. The presence of plastic deformation observed both in the zircons and whole rock implies that the deformation in the syenite was likely triggered by increased stress within the magma system.

Abbreviations

CL	Cathodoluminescence
EBSD	Electron backscattered diffraction
EMP	Electron microprobe
BSE	Backscattered electron
SEM	Scanning electron microscope
FE-SEM	Field emission scanning electron microscope
SEES	School of Earth and Environmental Sciences
SNU	Seoul National University
KBSI	Korea Basic Science Institute
BC	Band contrast
GROD	Grain reference orientation deviation
REE	Rare earth element
SHRIMP	Sensitive high-resolution ion microprobe

Acknowledgements

We thank Min-Ji Jung and Shinae Lee for their assistance in zircon sample preparation. Constructive comments and suggestions from journal reviewers improved the manuscript significantly.

Author contributions
ACSC designed the research. SC and ACSC wrote the manuscript. SC, KY, and HJ conducted the experiments. All authors contributed to the interpretation of the results and have read and approved the final manuscript.

Funding
This work was jointly supported by the National Research Foundation of Korea (NRF) grant funded by the Korean government (MSIT) (2021R1A2C1003363) and a KBSI grant (C380100) awarded to Albert Chang-sik Cheong, by a grant of the "National Research Council of Science & Technology (NST) –KBSI" Postdoctoral Research Fellowship for Young Scientists at KBSI to Seungsoon Choi, and by the National Research Foundation of Korea (NRF: 2022R1A5A1085103) to Haemyeong Jung.

Availability of data and materials
All data generated or analyzed during this study are included in this published article [and its additional files].

Declarations

Competing interests
The authors declare that they have no competing interests.

Received: 30 October 2023 Accepted: 8 March 2024
Published online: 18 March 2024

References

Cheong ACS, Kim Y, Jung MJ, Jeong YJ, Kim GB, Sohn YK. Long-lived shallow crustal magma reservoirs beneath Ulleung Island volcano (South Korea) and their rejuvenation recorded in zircon. Gondwana Res. 2024. https://doi.org/10.1016/j.gr.2023.12.006.
Cheong W, Cho M, Kim Y. An efficient method for zircon separation using the gold pan. J Petrol Soc Korea. 2013. https://doi.org/10.7854/JPSK.2013.22.1.063.
Cherniak DJ, Watson EB. Diffusion in zircon. Rev Mineral Geochem. 2003. https://doi.org/10.2113/0530113.
Claves SR, Deal A. Orientation dependence of EBSD pattern quality. Microsc Microanal. 2005. https://doi.org/10.1017/S1431927605507347.
Corfu F, Hanchar JM, Hoskin PWO, Kinny P. Atlas of zircon textures. Rev Mineral Geochem. 2003. https://doi.org/10.2113/0530469.
Ewing RC, Lutze W, Weber WJ. Zircon: A host phase for the disposal of weapons plutonium. J Mater Res. 1995. https://doi.org/10.1557/JMR.1995.0243.
Geisler T. Isothermal annealing of partially metamict zircon: Evidence for a three-stage recovery process. Phys Chem Miner. 2002. https://doi.org/10.1007/s00269-002-0249-3.
Geisler T, Schaltegger U, Tomaschek F. Re-equilibration of zircon in aqueous fluids and melts. Elements. 2007. https://doi.org/10.2113/gselements.3.1.43.
Hanchar JM, Rudnick RL. Revealing hidden structures: the application of cathodoluminescence and back-scattered electron imaging to dating zircons from lower crustal xenoliths. Lithos. 1995. https://doi.org/10.1016/0024-4937(95)00022-4.
Hoskin PWO. Patterns of chaos: fractal statistics and the oscillatory chemistry of zircon. Geochim Cosmochim Acta. 2000. https://doi.org/10.1016/S0016-7037(00)00330-6.
Hoskin PWO, Black LP. Metamorphic zircon formation by solid-state recrystallization of protolith igneous zircon. J Metamorph Geol. 2000. https://doi.org/10.1046/j.1525-1314.2000.00266.x.
Huijsmans JR, Hamers M, Drury MR, Lee JKW. Recrystallisation and trace-element mobility in zircons: Implications for U-Pb dating. Minerals. 2022. https://doi.org/10.3390/min12121489.
Kim GB, Cronin SJ, Yoon WS, Sohn YK. Post 19 ka B.P. eruptive history of Ulleung Island, Korea, inferred from an intra-caldera pyroclastic sequence. Bull Volcanol. 2014. https://doi.org/10.1007/s00445-014-0802-1.
Kovaleva E, Klötzli U, Habler G, Huet B, Guan Y, Rhede D. The effect of crystal-plastic deformation on isotope and trace element distribution in zircon: combined BSE, CL, EBSD, FEG-EMPA and NanoSIMS study. Chem Geol. 2017. https://doi.org/10.1016/j.chemgeo.2016.12.030.
Nasdala L, Lengauer CL, Hanchar JM, Kronz A, Wirth R, Blanc P, Kennedy AK, Seydoux-Guillaume AM. Annealing radiation damage and the recovery of cathodoluminescence. Chem Geol. 2002. https://doi.org/10.1016/S0009-2541(02)00152-3.
Piazolo S, Fontaine AL, Trimby P, Harley S, Yang L, Armstrong R, Cairney JM. Deformation-induced trace element redistribution in zircon revealed using atom probe tomography. Nat Commun. 2016. https://doi.org/10.1038/ncomms10490.
Poller U, Huth J, Hoppe P, Williams IS. REE, U, Th, and Hf distribution in zircon from Western Carpathian Variscan granitoids: a combined cathodoluminescence and ion microprobe study. Am J Sci. 2001. https://doi.org/10.2475/ajs.301.10.858.
Pidgeon RT, Nemchin AA, Hitchen GJ. Internal structures of zircons from Archaean granites from the Darling Range batholith: implications for zircon stability and the interpretation of zircon U-Pb ages. Contrib Mineral Petrol. 1998. https://doi.org/10.1007/s004100050422.
Précigout J, Ledoux E, Arbaret L, Spriet C. Porosity induced by dislocation dynamics in quartz-rich shear bands of granitic rocks. Sci Rep. 2022. https://doi.org/10.1038/s41598-022-10053-x.
Reddy SM, Timms NE, Trimby P, Kinny PD, Buchan C, Blake K. Crystal-plastic deformation of zircon: a defect in the assumption of chemical robustness. Geology. 2006. https://doi.org/10.1130/G22110.1.
Reddy SM, Timms NE, Hamilton PJ, Smyth HR. Deformation-related microstructures in magmatic zircon and implications for diffusion. Contrib Mineral Petrol. 2009. https://doi.org/10.1007/s00410-008-0331-z.
Rubatto D. Zircon: the metamorphic mineral. Rev Mineral Goechem. 2017. https://doi.org/10.2138/rmg.2017.83.09.
Rubatto D, Gebauer D. Use of cathodoluminescence for U-Pb zircon dating by ion microprobe: some examples from the Western Alps. In: Pagel M, Barbin V, Blanc P, Ohnenstetter D, editors. Cathodoluminescence in geosciences. Berlin Heidelberg New York: Springer; 2000. p. 373–400.
Stroh AN. A theory of the fracture of metals. Adv Phys. 1957. https://doi.org/10.1080/00018735700101406.
Timms NE, Kinny PD, Reddy SM, Evans K, Clark C, Healy D. Relationship among titanium, rare earth elements, U-Pb ages and deformation microstructures in zircon: implications for Ti-in-zircon thermometry. Chem Geol. 2011. https://doi.org/10.1016/j.chemgeo.2010.10.005.
Timms NE, Reddy SM, Gerald JDF, Green L, Muhling JR. Inclusion-localised crystal-plasticity, dynamic porosity, and fast-diffusion pathway generation in zircon. J Struct Geol. 2012. https://doi.org/10.1016/j.jsg.2011.11.005.
Vonlanthen P, Gerald JDF, Rubatto D, Hermann J. Recrystallization rims in zircon (Valle d'Arbedo, Switzerland): An integrated cathodoluminescence, LA-ICP-MS, SHRIMP, and TEM study. Am Miner. 2012. https://doi.org/10.2138/am.2012.3854.
Weertman J. Zener-Stroh crack, Zener-Hollomon parameter, and other topics. J Appl Phys. 1986. https://doi.org/10.1063/1.337236.

Publisher's Note